metals

MDPI

Article

Study on the Electromigration Organization and Mechanical Properties of Sn2.5Ag0.7Cu0.1RE/Cu Solder Joints

Yuming Wang [1], Keke Zhang [1,2,*], Chao Zhang [3], Fupeng Huo [4] and Yijie Gao [1]

[1] School of Materials Science and Engineering, Henan University of Science and Technology, Luoyang 471000, China; wym520105@163.com (Y.W.); gaoyj98@163.com (Y.G.)
[2] Key Laboratory of Nonferrous Metals Science and Processing Technology in Henan Province, School of Materials Science and Engineering, Henan University of Science and Technology, Luoyang 471000, China
[3] School of Mechanical and Electrical Engineering, Luo Yang Polytechnic, Luoyang 471000, China; zcwilly@126.com
[4] Flexible 3D System Integration Laboratory, The Institute of Science and Industrial Research, Osaka University, 8-1 Mihogaoka, Ibaraki City 567-0047, Osaka, Japan; huofp@sanken.osaka-u.ac.jp
* Correspondence: zhkeke@haust.edu.cn

Abstract: In this study, we designed and manufactured an ideal electromigration testing device for soldering joints to solve the reliability problems caused by temperature and current density changes in the electromigration processes of micro solder joints. We analyzed the effects of temperature and current density on the electromigration β-Sn (single-crystal β-Sn grain) of Sn2.5Ag0.7Cu0.1RE/Cu solder joints, the relationship between the grain orientation and interfacial IMC (intermetallic compound) growth of Sn2.5Ag0.7Cu0.1RE/Cu solder joints, and the mechanical properties of solder joints. The results showed that the angle θ between the c-axis of the β-Sn grain and the current direction for the Sn2.5Ag0.7Cu0.1RE/Cu solder joint gradually decreased to 8.2° when the temperature increased to 150 °C, which accelerated the diffusion of Cu atoms and Cu substrate dissolution. The recrystallization and grain growth of Cu_6Sn_5 (An intermetallic compound formed by the fusion of copper and tin in a ratio of six to five) grains in the anode region promoted electromigration polarity. Compared with the initial state, the shear strength decreased to 11 MPa, a decrease of 61.3%, the fracture position shifted from the top of the IMC at the cathode interface to the root of the IMC at the cathode interface, and the fracture mode changed from ductile fracture to brittle fracture. With an increase in the current density to 1.1×10^4 A/cm^2, θ decreased to 3.2°. In addition, we observed the recrystallization of Cu_6Sn_5 grains in the anode region and an increase in the grain length and diameter to 6.8–31.9 μm, which further promoted electromigration polarity. Compared with the initial state, the shear strength decreased by 72.5% to 7.8 MPa, and the fracture position shifted from the top of the IMC at the cathode interface to the root of the IMC at the cathode interface. Additionally, the fracture mode changed from ductile to brittle fracture.

Keywords: Sn2.5Ag0.7Cu0.1RE soldering metal; electromigration; temperature; current density; intermetallic compounds; grain orientation; shear strength

Received: 16 December 2024
Revised: 6 January 2025
Accepted: 14 January 2025
Published: 16 January 2025

Citation: Wang, Y.; Zhang, K.; Zhang, C.; Huo, F.; Gao, Y. Study on the Electromigration Organization and Mechanical Properties of Sn2.5Ag0.7Cu0.1RE/Cu Solder Joints. *Metals* **2025**, *15*, 75. https://doi.org/10.3390/met15010075

1. Introduction

With the continuous development of microelectronic products towards miniaturization and multi-functionalization, the scale of micro–nano connection technology is shrinking, thereby increasing the number of microsoldering joints and the current density carried by them. This situation is leading to electromigration [1–3], a phenomenon in which charges move through a medium and are affected by temperature and current density, thus affecting

the performance and reliability of semiconductor materials and electronic devices [4–9]. Therefore, it is important to understand the effects of temperature and current density on electromigration. Chen et al. [10] observed significant electromigration in the local area above the critical value of current density caused by the current concentration effect in solder joints with low current density. To avoid the current concentration effect, Li et al. [11] designed an in situ constant temperature electromigration test for triangular-prism-shaped Cu/Sn3.0Ag0.5Cu/Cu solder joints. At a temperature of 120 °C and a current density of 7×10^3 A/cm^2, obvious electromigration polarity was observed, which demonstrated that the threshold current density of electromigration occurred or was correlated with the external (ambient) temperature. Chellvarajoo et al. [12] also found that temperature is an important factor affecting electromigration, and that the polarity of electromigration becomes more significant as the temperature increases. Han et al. [13] found that with an extension of the current loading time, the solder joint transitioned from ductile fracture to brittle fracture, with fracture sites mostly occurring in the cathode region. Zuo et al. [14] compared the electromigration phenomenon of Cu/Sn3.0Ag0.5Cu/Cu solder joints at temperatures of 100 °C and 25 °C and found that the migration rates of Cu and Sn atoms varied, resulting in large differences in the timing of electromigration polarity mounds. This result indicated the existence of an incubation period for the electromigration polarity effect of microelectron connection solder joints. Wang et al. found that with an increase in temperature, the electromigration rate increased and tended to become saturated within a certain temperature range [15–18]. Hsu, Y.C. et al. [19] studied the electromigration behavior at different current densities in the temperature range of 80–120 °C and measured the corresponding critical current densities of 4.3×10^4 A/cm^2, 3.2×10^4 A/cm^2, and 1.4×10^4 A/cm^2 at higher temperatures. The results indicated that the current densities needed for electromigration to occur were reduced at higher temperatures, with electromigration itself becoming more commonplace. Jiang Nan et al. [20–22] found that with an increase in the current density, the c-axis angles of Sn grains decreased. When the angle θ between the current direction and the c-axis of the Sn grain was 90°, the electromigration behavior weakened. When the angle θ between the current direction and the c-axis of the Sn grain was 0°, the Cu atoms spread outward along the gap of the c-axis for the Sn particle, which accelerated the appearance of electromigration. Zhang found that large grains in polycrystalline β-Sn are the most dominant grains in affecting electromigration [23], so this paper focuses on large single-crystal β-Sn grains.

In summary, although there is a preliminary understanding of the correlation between temperature and current density and electromigration of lead-free soldered joints, the development of the research is constrained by the single means of the relevant research equipment. This paper takes Sn2.5Ag0.7Cu0.1RE/Cu soldered joints as the research object, designs and manufactures electromigration test devices under different temperatures and current densities, and observes and analyzes the effects of soldered joints' temperatures and current densities on the IMC (intermetallic compound) and mechanical properties of the interface of electromigration and at the same time also observes and analyzes the relationship between single-crystalline β-Sn grain orientation and the interface IMC mechanism and the reliability of solder joints. The study provides a key foundation for the design and reliability of solder joints. It provides theoretical and experimental basis for the reliability design and manufacture of high-reliability lead-free soldering material soldered joints, which is of great significance to the manufacture of electronic information industry.

2. Materials and Methods

2.1. Preparation of the Soldering Metal

As shown in Figure 1, Sn2.5Ag0.7Cu0.1RE powder was obtained by mixing Sn, Ag, and Cu powders with purities greater than 99.9% and rare earth (RE) powder with main contents of Ce and La in a certain ratio [24]. These powders were evenly mixed in a planetary ball mill at a speed of 180 r/min for 8 h. The mixed soldering metal powder was then pressed into a cylindrical shape with a diameter of 20 mm and sintered in a vacuum furnace at 180 °C for 2 h to obtain the composite soldering metal required for the test. Finally, the composite soldering metal was rolled into a thin sheet of 1 mm × 0.5 mm, and a copper plate with a mass fraction of 99.9% was selected as the soldering base metal.

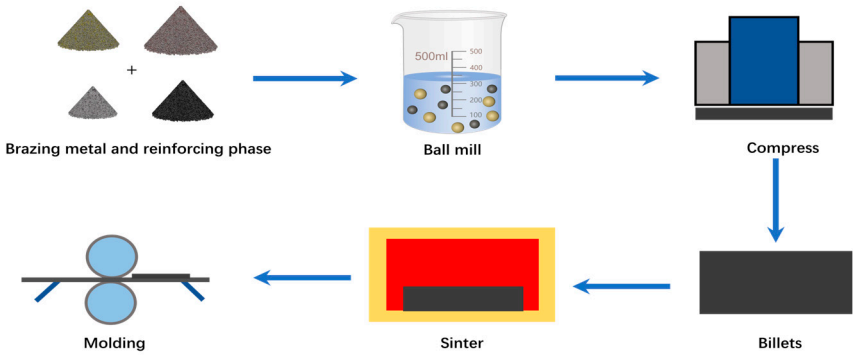

Figure 1. Flow chart of soldering material preparation.

2.2. Soldering Test

The solder joints in this test were integrated for easy disassembly and assembly and partially butted to eliminate changes in the direction of heat conduction. A schematic diagram of the solder joints is shown in Figure 2 [25].

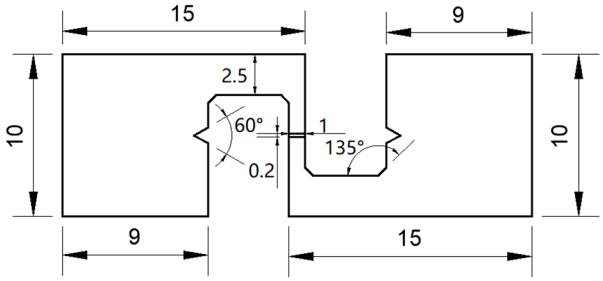

Figure 2. Schematic diagram of the solder joint specimen (all units on the diagram are in mm).

After grinding and cleaning the surface to be soldered and the soldering flake, drop the appropriate amount of CX600 commercial water-cleaning flux into it, send it into the vacuum soldering furnace, and obtain the soldered joint after cooling. The test soldering temperature is 270 °C, the holding time is 210 s, and the cooling method is air cooling [26].

2.3. Design, Manufacture, and Testing of Electric Relocation Device

To meet the electromigration test conditions of solder joints in the oil bath environment, the apparatus was composed of an electromigration energizing device and a temperature field test chamber. The working principle of the designed and manufactured electromigration test device is shown in Figure 3. The device also included a DC-regulated power supply, an energizing fixture, and a temperature field test chamber. To reduce the influence of contact resistance on the electromigration test, we used a single strand of pure Cu wire, which was filled with Sn. Then, the bolts fixed with the electromigration sample were

spaced to expand the contact area with the soldering joint. The temperature field test chamber was able to meet the test conditions in the oil bath environment. The electromigration test was conducted under a variety of temperature fields in the constant temperature environment, with parameters set using a temperature measurement and control panel. After the electromigration test, the specimen was air-cooled for half an hour and then disassembled. The specific experimental parameters are shown in Table 1.

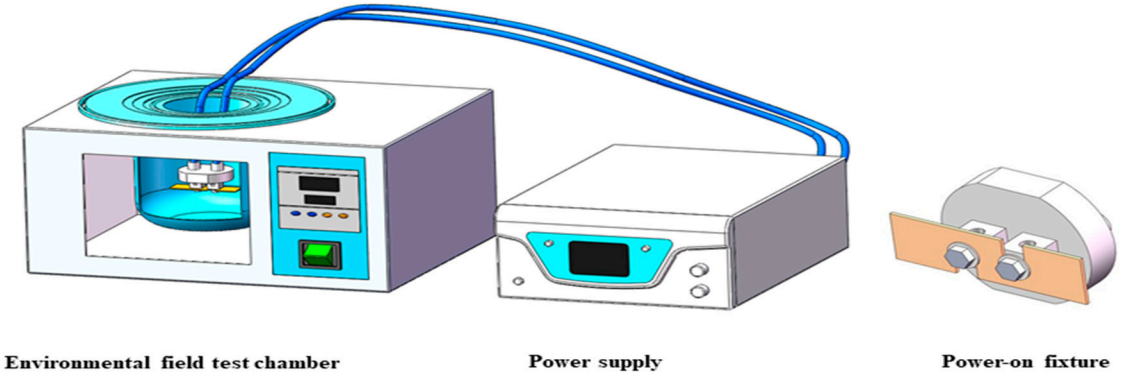

Figure 3. Electromigration devices.

Table 1. Technical parameters for studying the influence of temperature and current density on electromigration.

Research Factor	Current Density (A/cm^2)	Energizing Time (h)	Temperature (°C)
Influence of Temperature	7×10^3	100	70 110 150
Influence of Current Density	5×10^3 8×10^3 1.1×10^4	100	110

2.4. Determining the Microstructure and Mechanical Properties of Solder Joints

The prepared electromigration specimens were mounted, sanded, polished, and corroded with a 4% hydrochloric acid alcohol mixture for 10 s [27]. Subsequently, the specimens were placed in a JSM-IT100 (JEOL Ltd., Tokyo, Japan) tungsten filament scanning electron microscope for observations, and EBSD (Carl Zeiss AG, Oberkochen, Germany) was used to analyze the microstructure and phase [28]. The SEM photos of the IMC (intermetallic compound) interface were imported into the AutoCAD software 2021, and the area and length of certain areas were randomly measured. The average thickness of the IMC at the interface of the region was obtained using the equal area method [29]. To ensure the reliability of the data, five areas were randomly selected for area and length measurements.

The tensile test used a UTM2503 micro-tensile testing machine (Jinan Kesheng Testing Equipment Co., Ltd., Jinan, China) and was carried out using ±0.5% test force accuracy and a 0.5 mm/min tensile rate. Three specimens were selected for tensile testing under each test parameter, and the average shear strength of the three specimens was taken as the shear strength of the solder joint under this test parameter [30]. A JSM-IT100 tungsten filament scanning electron microscope was used to observe the shear and cut of the solder joint, and the necessary composition analysis was carried out via energy spectroscopy.

3. Results and Discussion

3.1. Electromigration Microstructure of Sn2.5Ag0.7Cu0.1RE/Cu Solder Joints

The electromigration microstructure of the Sn2.5Ag0.7Cu0.1RE/Cu solder joint is shown in Figure 4a. This solder joint was composed of a base metal Cu substrate, an interfacial IMC layer, and a soldering seam zone composed of primary phase β-Sn and eutectic structures. These eutectic structures included granular β-Sn + Cu_6Sn_5, needle-β-Sn + Ag_3Sn binary eutectic structures, and β-Sn + Cu_6Sn_5 + Ag_3Sn ternary eutectic structures [31–33]. IMC was mainly composed of scallop-like Cu_6Sn_5 (An intermetallic compound formed by the fusion of copper and tin in a ratio of six to five). Figure 4b shows the high-power SEM in Region A, while the component analysis results in Region B are shown in Figure 4c. Region B was mainly composed of Sn and Cu. The EBSD phase diagram of the anode region presented in Figure 4d indicates that the interfacial IMC was composed of many Cu_6Sn_5 phases and a small amount of Cu_3Sn (An intermetallic compound formed by the fusion of copper and tin in a ratio of three to one) phases. This research focused on the cathode and anode interface of the solder joint since electromigration primarily affects atomic migration, yielding changes in the morphology of the IMC at the interface between the cathode and anode of the solder joint. In addition, void cracks in the IMC can occur at the interface of the cathode region [34,35].

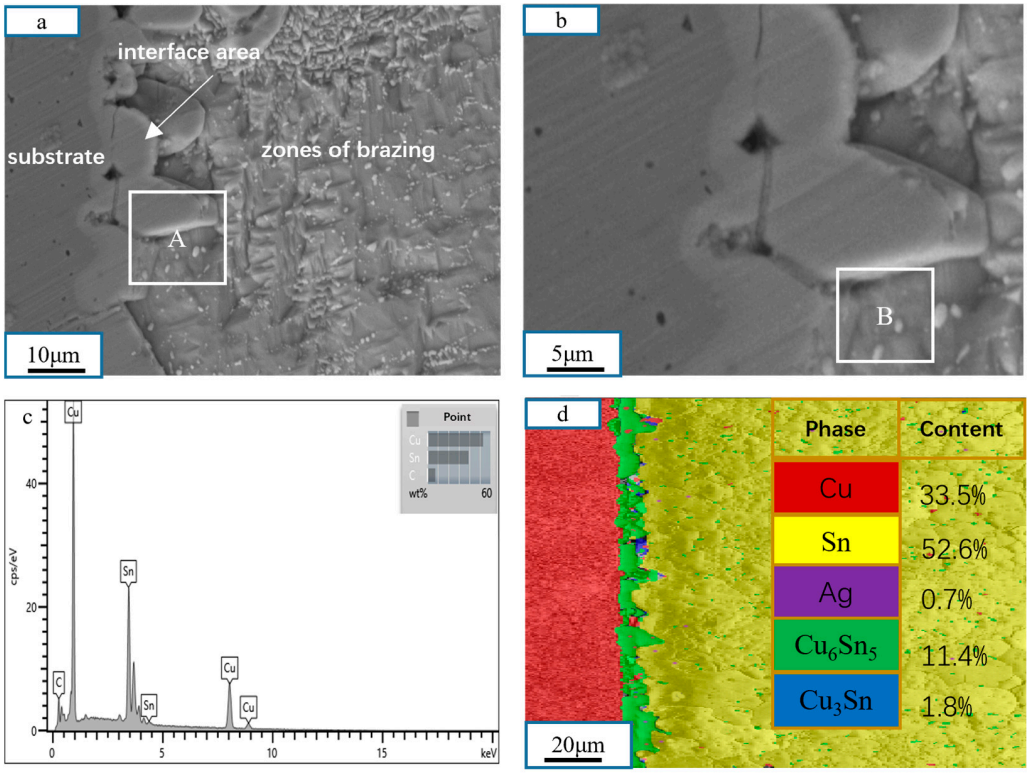

Figure 4. Electromigration microstructure of the Sn2.5Ag0.7Cu0.1RE/Cu solder joint: (**a**) anode region, (**b**) high-power SEM image of Region A in (**a**), (**c**) composition analysis of Region B in (**b**), (**d**) analysis of the EBSD phase diagram of the anode region.

3.1.1. Effect of Temperature on Tissues

Figure 5 shows an IMC (intermetallic compound) microstructure diagram and EBSD orientation diagram of the cathode region interface under different temperatures with a current density of 7 × 10^3 A/cm^2 and a loading completion time of 100 h for Sn2.5Ag0.7Cu0.1RE0.05Ni-GNSs/Cu solder joints. As shown in Figure 5(a1–c1), the interface IMC in the cathode region of the solder joint (temperature: 70 °C) was symmetrical,

while that at both ends was mainly a continuously distributed "scallop-like" Cu_6Sn_5 layer. In addition, no Cu_3Sn formation or obvious electromigration polarity was observed. When the temperature increased from 110 °C to 150 °C, the thickness of the Cu_6Sn_5 layer in the anode region of the interface increased significantly, with the shape beginning as wave-like and then fusing into a coarse lamellar sheet. The thickness of the Cu_6Sn_5 layer at the interface of the cathode region decreased, and the number of Kirkendal voids affected by diffusion in the Cu_3Sn layer increased.

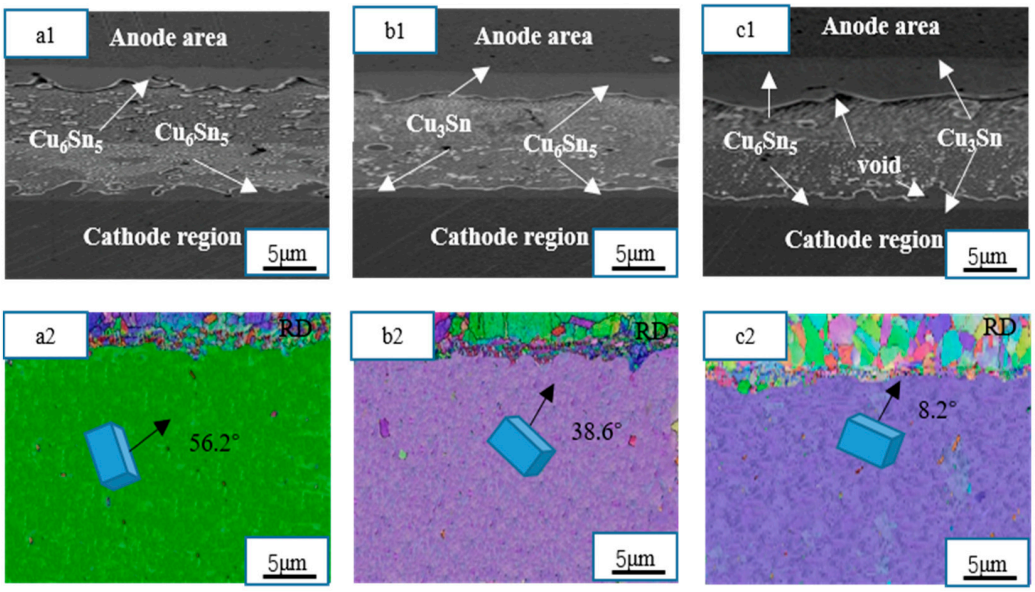

(**a**) 70 °C (**b**) 110 °C (**c**) 150 °C

Figure 5. Microstructure (**a1**–**c1**) and corresponding EBSD orientation maps (**a2**–**c2**) of the IMC boundary figure in the cathode and anode regions of Sn2.5Ag0.7Cu0.1RE/Cu solder joints at a current density of 7×10^3 A/cm^2 and a loading completion time of 100 h under oil bath temperatures of 70 °C, 110 °C, and 150 °C.

The EBSD orientation diagram in Figure 5(a2) shows that for the anode region at 70 °C with a larger β, the angle θ between the c-axis of the -Sn grain and the current direction is 56.2°. The Cu atoms mainly come from Cu substrate dissolution. The Cu_6Sn_5 grain orientation is also more chaotic, with a grain diameter of 3.2–8.8 μm. In addition, this figure shows that the proportion has a relatively large-angle grain boundary with very large energy and that the Cu_6Sn_5 faced difficulties growing under a temperature of 70 °C. Figure 5(b2) shows the EBSD orientation of the anode region at 110 °C. Here, with an increase in temperature for β, the angle θ between the c-axis of the C-Sn grain and the current direction becomes 38.6°. The Cu atoms are mainly diffused through Cu substrate dissolution and the migration of Cu atoms in the cathode region, resulting in the grain size of Cu_6Sn_5 on the side of the Cu substrate growing significantly and flattening compared with the results under a temperature of 70 °C. The Cu_6Sn_5 orientation also becomes more chaotic at this time, and the Cu_6Sn_5 grain diameter varies from 7.5 μm to 25.4 μm. Figure 5(c2) shows an EBSD orientation diagram of the anode region at 150 °C. With an increase in temperature to 150 °C, the angle θ between the c-axis and the current direction of the β-Sn grain decreased to 8.2°. The diffusion of Cu atoms subsequently intensified, yielding a further increase in the grain size of Cu_6Sn_5 on the side close to the Cu substrate and an obvious preferential orientation in the grain orientation. The newly formed Cu_6Sn_5 grains near the soldering seam further increased, and the grain orientation became more chaotic. In addition, the Cu_6Sn_5 grains coarsened, and the diameter increased to 7.8–32.7 μm, indicating that with an increase in temperature, the angle θ between the

c-axis of the β-Sn grain and the current direction decreased. Then, the electromigration phenomenon became increasingly obvious, Cu substrate dissolution and the migration of atoms in the cathode region to the anode region, as well as the recrystallization and growth of Cu_6Sn_5 grains in the anode region. This finding is in agreement with Shen et al. who suggested that Cu-Sn IMC grows very fast during electromigration for Sn grains with β-Sn grains with c-axis θ angle less than 25° [36]. In summary, as temperature rises, under the dual influence of electron wind and temperature, atomic thermal motion intensifies, the diffusion coefficient increases, and the diffusion rate accelerates. During electromigration, the anode acts as the recipient of metal ions. Higher temperatures enable more metal atoms to surmount the energy barrier, diffusing from the cathode to the anode and depositing there, thus increasing the thickness of the intermetallic compound (IMC) at the anode.

At the cathode, metal atoms continuously migrate to the anode due to electromigration, and the elevated temperature further expedites this process. This leads to a more rapid depletion of metal atoms at the cathode, inhibiting the growth of the cathode IMC and reducing its thickness.

Furthermore, grain boundaries, which serve as rapid diffusion pathways for atoms, become more influential as temperature increases. The anode region likely harbors a relatively high density of high-angle grain boundaries. The temperature increase enhances the atomic diffusion rate along these grain boundaries, allowing more atoms to rapidly diffuse through them into the IMC growth region. This accelerates IMC growth and contributes to an increase in anode IMC thickness.

Conversely, the cathode's microstructure may impede atomic diffusion. As temperature increases and anode-side atomic diffusion intensifies, relatively fewer atoms are available for IMC growth at the cathode, resulting in a decrease in cathode IMC thickness.

Figure 6: Sn2.5Ag0.7Cu0.1RE with a current density of 7×10^3 A/cm^2 and a loading completion time of 100 h. Figure 6a shows that the asymmetric growth of the cathode and anode IMC is relatively flat when the temperature is between 70 °C and 110 °C. Moreover, the increase rate for total IMC thickness and the difference in IMC thickness between the cathodes was relatively stable at this stage. In addition, the increase and decrease rates of the IMC between the total thickness of the cathode and the IMC thickness increased significantly when the temperature was between 110 °C and 150 °C. As shown in Figure 6b, the linear increase in the difference between the total thickness of the IMC and the current thickness of the IMC increased at this stage, at which time IMC growth was in its expansion phase. In summary, with an increase in temperature, electromigration became more obvious and intense under the dual effects of electronic wind and temperature.

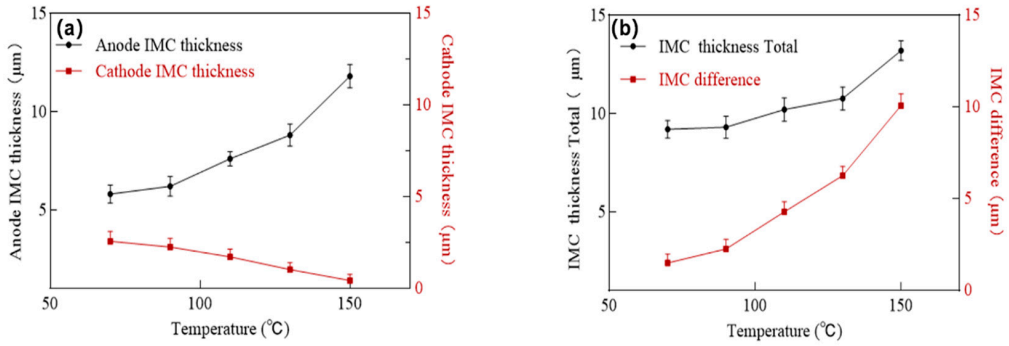

Figure 6. Under the conditions of a current density of 7×10^3 A/cm^2, and a loading completion time of 100 h at oil bath temperatures of 70 °C, 110 °C, and 150 °C. (**a**) The thickness of the intermetallic compound (IMC) in the cathode and anode regions of the Sn2.5Ag0.7Cu0.1RE/Cu solder joint. (**b**) The difference between the sum of the IMC thicknesses of the cathode and anode.

3.1.2. Effect of Current Density on Tissues

Figure 7 presents the IMC boundary diagram and EBSD orientation diagram for the Sn2.5Ag0.7Cu0.1RE/Cu solder joint in the cathode and anode regions under different current densities at 110 °C and a loading completion time of 100 h. Figure 7(a1) shows the current density of 5×10^3 A/cm^2. The interface between the Cu substrate and the cathode and anode regions formed a continuous scallop-like Cu_6Sn_5 intermetallic compound and a thin, light gray layer of the compound Cu_3Sn. In addition, the interface between the cathode and anode IMC was in good condition, with no defects such as cracks or holes. Figure 7(b1) shows that the IMC interface at a current density of 8×10^3 A/cm^2 changed significantly compared to the IMC interface at a current density of 5×10^3 A/cm^2. The thickness of the IMC at the interface of the anode region also increased significantly, presenting a thick slat, as did the light gray Cu_3Sn compound between the Cu_6Sn_5 and Cu substrate. Conversely, the thickness of the IMC in the cathode region decreased as the morphology changed to thin slats with cavity cracks. Figure 7(c1) shows that under a current density of 1.1×10^4 A/cm^2, the thickness of the interface IMC in the anode region of the solder joint increased sharply and the morphology resembled a thick slat. Additionally, the Cu_3Sn that formed between the Cu_6Sn_5 and Cu substrate in the anode region thickened further, while the thickness of the interface IMC in the cathode region decreased. IMC at the interface in the cathode region presented as a thin strip, and the crack grew further.

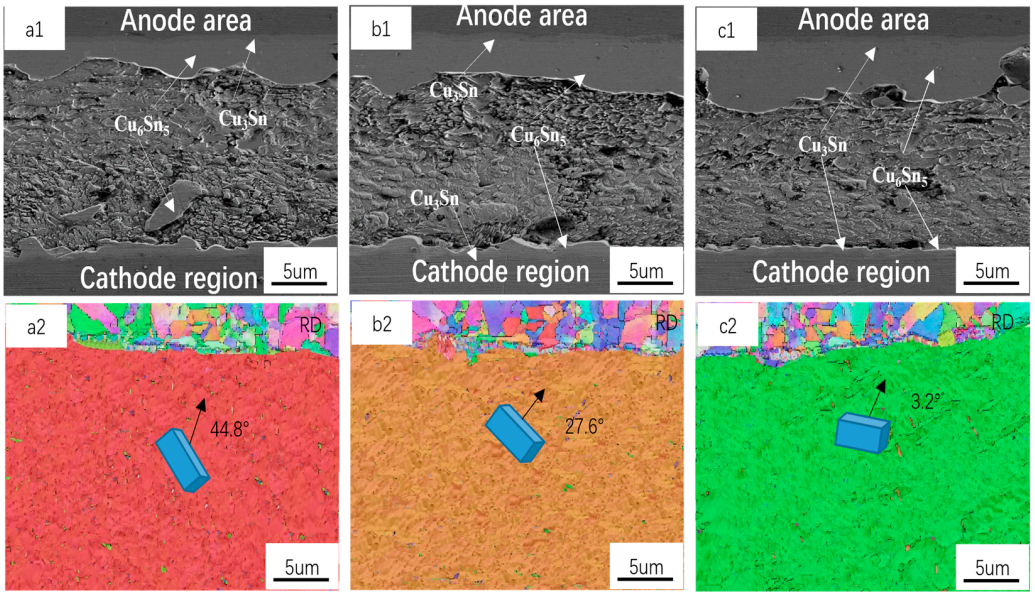

(**a**) 5 × 10³ A/cm² (**b**) 8 × 10³ A/cm² (**c**) 1.1 × 10⁴ A/cm²

Figure 7. Microstructure (**a1–c1**) and corresponding EBSD orientation maps (**a2–c2**) for the IMC boundary in the cathode area of Sn2.5Ag0.7Cu0.1RE/Cu solder joints at an oil bath temperature of 110 °C; a loading completion time of 100 h; and current densities of 5×10^3 A/cm^2, 8×10^3 A/cm^2, and 1.1×10^4 A/cm^2.

Figure 7(a2–c2) shows the EBSD crystal structure orientation of β-Sn grains in the anode region at different current densities (see Figure 7(a2)). The angle θ between the c-axis of the β-Sn grain and the current direction indicates that Cu atoms mainly diffused through Cu substrate dissolution at a large angle of 44.8°. The grain orientation of Cu_6Sn_5 then became more chaotic, with a grain diameter of 3.8–9.6 μm, a high proportion of large-angle grain boundaries, and large grain boundary energy. When the current density was 8×10^3 A/cm^2, as shown in Figure 7(b2), the angle θ between the c-axis of single crystal β-Sn and large grain β-Sn was 27.6°. Here, Cu atoms mainly diffused through Cu substrate dissolution and the migration of Cu atoms in the cathode region, resulting in a grain size of

Cu_6Sn_5 near the Cu substrate higher than 5×10^3 A. The newly formed Cu_6Sn_5 grains near the soldering seam side were small, and the grain orientation was relatively messy, with a Cu_6Sn_5 grain diameter of 6.2–22.4 μm. When the current density was 1.1×10^4 A/cm^2, as shown in Figure 7(c2), the angle θ between the c-axis and the current direction of the β-Sn die of the solder joint further reduced to 3.2°. The diffusion of Cu atoms then intensified, further increasing the grain size of Cu_6Sn_5 on the side near the Cu substrate, with an obvious preferential orientation in the grain direction. The newly formed Cu_6Sn_5 grains near the soldering seam also increased further with a chaotic grain orientation. Additionally, the Cu_6Sn_5 grains gradually coarsened—the diameter increased from 6.8 μm to 31.9 μm. Therefore, the current density of the solder joint was $\geq 8 \times 10^3$ A/cm^2 under a 100 h oil bath at a temperature of 110 °C. In summary, with an increase in current density, the angle θ between the c-axis of the β-Sn grains and the current direction decreased, Cu substrate dissolution and the migration of Cu atoms from the cathode region to the anode region. This phenomenon also led to the recrystallization and grain growth of Cu_6Sn_5 grains in the anode region, thickening of the interface IMC, and gradual thinning of the cathode until failure. This finding is in agreement with Fu et al. who suggested that when the c-axis of Sn grains is aligned with the current direction, the intermetallic compound layer is thicker at the anode and almost absent at the cathode [21]. In summary, as the current density escalates, the force of the electron wind strengthens, exacerbating the electromigration phenomenon. The electron wind, flowing from the cathode to the anode, exerts a drag force on metal atoms. At relatively high current densities, an increased number of metal atoms, such as Cu atoms, migrate from the cathode to the anode under the influence of the electron wind. At the anode, these additionally migrated atoms supply more materials for the growth of intermetallic compounds (IMC), contributing to an augmentation in the thickness of anode IMC.

Conversely, the cathode experiences a substantial loss of atoms, resulting in an insufficient number of atoms to sustain IMC growth. This leads to a deceleration of IMC growth, and in some instances, partial decomposition, ultimately culminating in failure.

On the other hand, the anode region is likely to have a relatively high density of high-angle grain boundaries. Under the effect of an electric field, atomic diffusion along these grain boundaries is accelerated. This allows more atoms to rapidly diffuse through the grain boundaries into the IMC growth region, expediting the growth of anode IMC and increasing their thickness.

In comparison, the grain boundary structure in the cathode region may be less conducive to rapid atomic diffusion. Alternatively, at high current densities, a large number of atoms at the grain boundaries are extracted, constraining the growth of cathode IMC and ultimately causing failure.

Figure 8 shows the IMC thickness of the cathode area on the Sn2.5Ag0.7Cu0.1RE/Cu solder joint with a current density of 7×10^3 A/cm^2 and a loading completion time of 100 h. Figure 8b shows that the increase rate for the total thickness of the cathode and the difference between the IMC thickness of the cathode and the IMC thickness of the anode was relatively stable at this stage. Additionally, as shown in Figure 8a, the growth of the IMC was stable in the range of 7×10^3 A/cm^2 to 8×10^3 A/cm^2. Figure 8b shows that the total IMC thickness did not change significantly. However, the linear increase rate for the IMC thickness difference grew at this stage, possibly due to an increase in the atomic and total migration rates. Figure 8a shows that the asymmetric growth of the cathode and anode IMC became relatively gentle between 8×10^3 A/cm^2 and 1.2×10^4 A/cm^2, with the material migration reaching its maximum at 1.2×10^4 A/cm^2. Here, the anode thickness was the largest, while the cathode thickness was the thinnest. In summary, with an increase in current density, electromigration became more obvious and intense, and the

growth of IMC on the anode side reached its maximum. Finally, fracture failure occurred at the IMC on the cathode side.

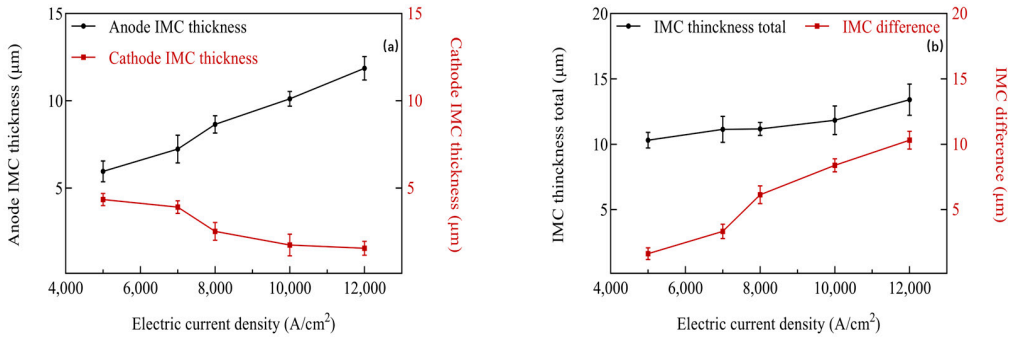

Figure 8. Under the conditions of a temperature of 110 °C, and a loading completion time of 100 h with 5×10^3 A/cm^2, 8×10^3 A/cm^2, and 1.1×10^4 A/cm^2 (**a**) The thickness of the intermetallic compound (IMC) in the cathode and anode regions of the Sn2.5Ag0.7Cu0.1RE/Cu solder joint. (**b**) The difference between the sum of the IMC thicknesses of the cathode and anode.

3.2. Electromigration Mechanical Properties of Sn2.5Ag0.7Cu0.1RE/Cu Soldering Joints

3.2.1. Effect of Temperature on the Electromigration Shear Strength of the Joint

Figure 9 shows the shear strength of the Sn2.5Ag0.7Cu0.1RE/Cu soldering joint at different temperatures. As shown in Figure 9, the shear strength of the solder joint decreased uniformly and relatively gently until the oil bath temperature reached 110 °C, after which the shear strength of the solder joint began to fluctuate slightly, and the decline rate increased. When the temperature increased to 150 °C, the shear strength of the solder joint was 11 MPa, which is 61.3% lower than that before energizing (28.4 MPa).

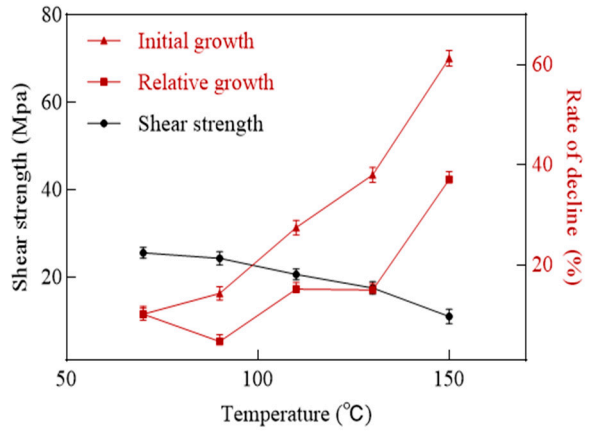

Figure 9. Effect of different temperatures on the shear strength of solder joints at a current density of 7×10^3 A/cm^2 and an electric loading time of 100 h.

Figure 10 presents the shear and cutting joints of Sn2.5Ag0.7Cu0.1RE/Cu soldering joints at different temperatures. With an increase in oil bath temperature, the number of dimples in the shear fractures decreased and the cleavage facets gradually increased and became smoother. As shown in Figure 10a, when the oil bath temperature was 70 °C, many dense spherical dimples and tear ridges appeared in the shear fracture. According to the spectroscopic analysis of Region A in Figure 10a, the shear fracture structure was dominated by the β-Sn phase, and the brittle phase with a small amount of Cu_6Sn_5 was ductile fractured. The fracture occurred at the edge of the dimple, forming a fracture fiber band through the inside of the grain, with the fracture occurring at the top of the cathode interface IMC. As shown in Figure 10b, when the oil bath temperature increased to 110 °C,

the shear cut of the solder joint was mainly composed of partial tear ridges and large cleavage facets. Additionally, the brittle phase of Cu_6Sn_5 in the B Region of Figure 10b increased, and a fracture occurred in the middle of the cathode interface IMC. Here, a tough–brittle mixed fracture mode could be observed. As shown in Figure 10c, when the oil bath temperature increased to 150 °C, the shear fracture was mainly composed of a large cleavage plane and a tear edge, with the whole fracture appearing relatively smooth. The fracture mode then changed from ductile to brittle fracture and the shear strength decreased very obviously. The compositional analysis of regions A, B and C is presented in Table 2.

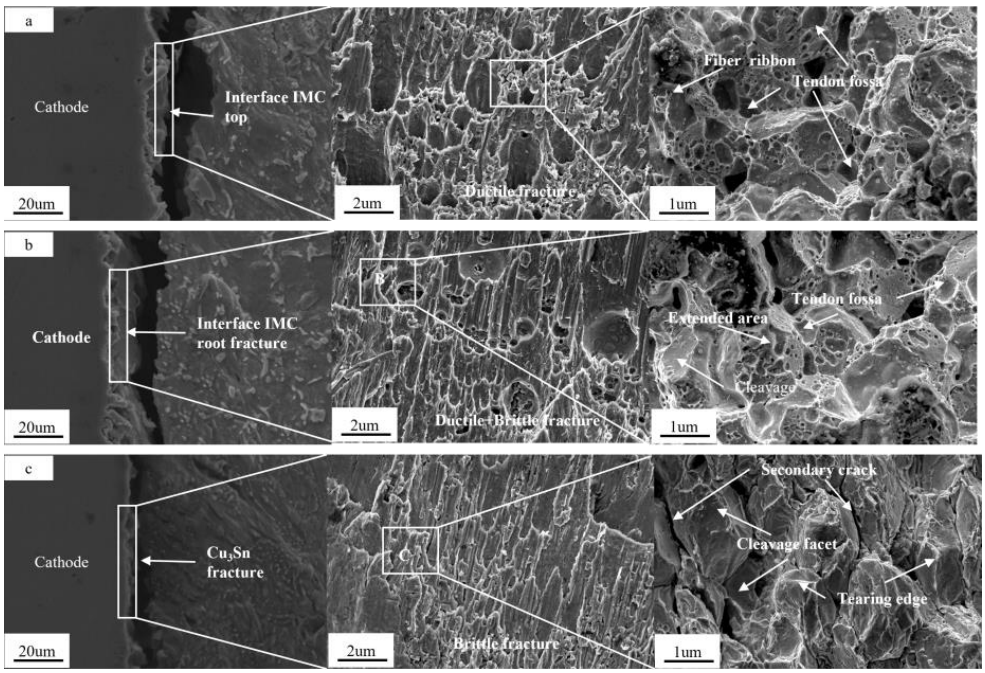

Figure 10. SEM images of the shear cut-off of the Sn2.5Ag0.7Cu0.1RE/Cu solder joint under different temperatures at a current density of 7×10^3 A/cm^2 and an electric loading time of 100 h: (**a**) oil bath temperatures of 70 °C, (**b**) 110 °C, and (**c**) 150 °C.

Table 2. EDS analysis of the shear and cut-off areas of solder joints at different oil bath temperatures (At.%).

Location	Sn	Ag
A	93.46	2.33
B	55.68	3.43
C	34.76	1.78

3.2.2. Effect of Current Density on the Shear Strength of the Joint

Figure 11 shows the electromigration shear strength of Sn2.5Ag0.7Cu0.1RE/Cu solder joints at different current densities. As shown in Figure 11, when the current density was less than 8×10^3 A/cm^2, the electromigration shear strength of the solder joint did not change significantly with an increase in current density until experiencing a small rapid decrease at 7×10^3 A/cm^2. When the current density exceeded 8×10^3 A/cm^2, the shear strength decreased significantly with an increase in the current density. When the current density reached 1.1×10^4 A/cm^2, the shear strength of the solder joint was 7.8 MPa, 72.5% lower than that before energizing (28.4 MPa).

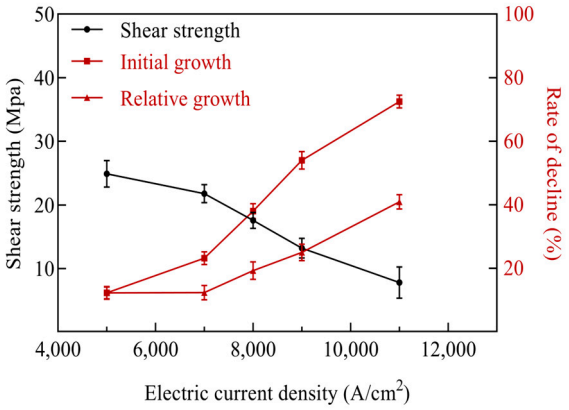

Figure 11. Effect of different current densities on the shear strength of solder joints at a temperature of 110 °C and electric loading time of 100 h.

Figure 12 presents the shear fracture under non-current density. Figure 12 indicates that with an increase in current density, the shear fracture gradually changed from many dense spherical dimples to cleavage facets supplemented by spherical dimples, followed by becoming flat and smooth. As shown in Figure 12a, when the current density was 5×10^3 A/cm^2, the shear fracture morphology presented dense spherical dimples, mainly small dimples, supplemented by large dimples, with a large number of tear ridges. According to the energy spectrum analysis of the A Region shown in Figure 12a, the shear fracture structure was dominated by a β-Sn phase with a small amount of the Cu_6Sn_5 phase, indicating ductile fracture. The fracture occurred at the top fracture near the cathode interface IMC. (As shown in Figure 13a) This is because, under a low current density of 5×10^3 A/cm^2, the electron wind is relatively weak. However, the solder joint at the top of the cathode, being directly exposed to the interface, has relatively active atoms that are more susceptible to the influence of the electron wind and thus prone to migration. The atomic migration leads to a decrease in the number of atoms in this area, gradually weakening the structure. Under the stress concentration induced by atomic migration, this site becomes a crack initiation locus. As electromigration proceeds, the crack propagates, ultimately resulting in fracture. As shown in Figure 12b, when the current density increased to 8×10^3 A/cm^2, the soldering joint shear cut was mainly composed of a larger spherical dimple and a smooth cleavage facet, while the fracture became flat. The energy spectrum analysis of the B Region in Figure 12b shows that the brittle phase of Cu_6Sn_5 increased, while the β-Sn phase of the shear fracture structure decreased, confirming that the fracture was located in the middle of the IMC at the cathode interface, with a mixed fracture mode presenting both toughness and brittleness (as shown in Figure 13b). This is because when the current density increases to 8×10^3 A/cm^2, the electron wind intensifies, causing a large number of atoms to migrate from the cathode to the anode. This leads to an exacerbated loss of atoms from the middle part of the cathode where Cu_6Sn_5 exists. Such atomic migration not only alters the chemical composition of Cu_6Sn_5 but also changes its microstructure, such as modifications in grain size and adjustments in grain boundary structure. The change in grain size may result in an increase in the grain boundary area. At the grain boundaries, atoms are arranged irregularly, with higher energy levels, making these areas prone to crack formation. As shown in Figure 12c, the current density increased to 1.1×10^4 A/cm^2 under the action of increasing Joule heating and electronic wind. At this juncture, the large spherical dimple within the shear fracture almost disappeared and a secondary crack appeared. The fracture was mainly composed of large cleavage facets and tear ridges, and the whole fracture looked relatively smooth and flat. Based on an EDS spectroscopic analysis of the C Region shown in Figure 12c, the structure of the

shear fracture was almost completely dissolved as the Cu_6Sn_5 phase, mainly the Cu_3Sn phase, and the fracture position shifted from the middle of the cathode interface IMC to the Cu_3Sn interface at the root of the cathode interface IMC. (As depicted in Figure 13c) This is attributed to the fact that when the current density reaches 1.1×10^4 A/cm^2, the effect of the electron wind becomes extremely strong. A substantial number of atoms continuously migrate away from the cathode, leading to a significant depletion of atoms at the root of the cathode where the Cu_3Sn phase is located. The structure of the Cu_3Sn phase is severely damaged, with the integrity of its crystal structure being lost and a substantial decline in the material's strength. The originally closely packed atomic structure becomes loose, rendering it unable to withstand external loads and internal stresses. The fracture pattern then changed from ductile fracture to brittle fracture, and the void density in the cathode region also increased, resulting in defects such as voids and cracks, which reduced the shear strength of the solder joint, significantly reducing its reliability. The fracture pathways of the solder joints at the three different current density stages are shown in Figure 13. The compositional analysis of regions A, B and C is presented in Table 3.

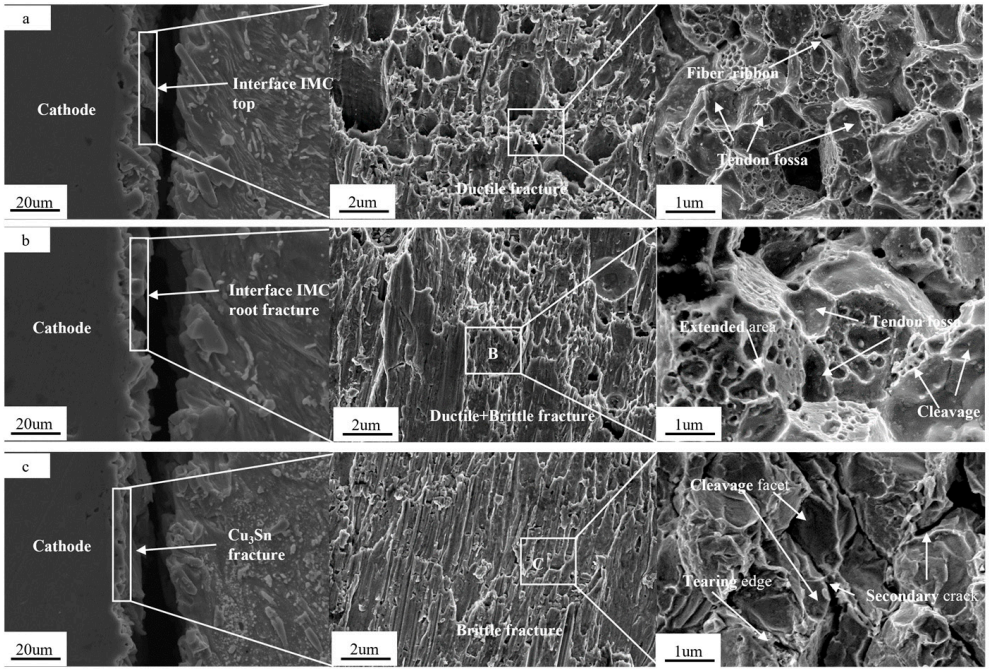

Figure 12. Scanning electron microscopy of the shear fracture of the Sn2.5Ag0.7Cu0.1RE/Cu solder joint under a 110 °C oil bath temperature and a 100 h electric loading time: (**a**) current density of 5×10^3 A/cm^2; (**b**) current density of 8×10^3 A/cm^2; (**c**) current density of 1.1×10^4 A/cm^2.

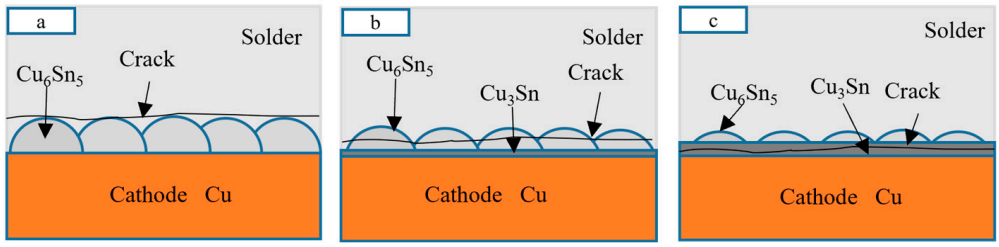

Figure 13. Schematic diagram of the shear fracture position of Sn2.5Ag0.7Cu0.1RE/Cu solder joints under different current densities under an oil bath temperature of 110 °C and electric loading time of 100 h: (**a**) current density of 5×10^3 A/cm^2; (**b**) 8×10^3 A/cm^2; and (**c**) 1.1×10^4 A/cm^2.

Table 3. EDS analysis of the shear and cut-off areas of the solder joints under different oil bath temperatures (At.%).

Location	Sn	Ag
A	94.77	2.33
B	57.46	3.24
C	25.56	1.02

Figure 12 shows the shear fracture under non-current density. Here, with an increase in current density, the shear fracture gradually changed from a large number of dense spherical dimples to cleavage facets supplemented by spherical dimples and then gradually became flat and smooth. As shown in Figure 12a, under a current density of 5×10^3 A/cm^2, the morphology of the shear fracture presented dense spherical dimples—mainly small dimples—supplemented by large dimples, with numerous tear ridges. According to the energy spectrum analysis of the A Region shown in Figure 12a, the shear fracture structure was dominated by the β-Sn phase with a small amount of the Cu_6Sn_5 phase, indicating ductile fracture. Additionally, the fracture occurred at the top near the cathode interface IMC. As shown in Figure 12b, when the current density increased to 8×10^3 A/cm^2, the soldering joint shear cut was mainly composed of a larger spherical dimple and a smooth cleavage facet, while the fracture became flat. The energy spectrum analysis of the B Region in Figure 12b shows that the brittle phase of Cu_6Sn_5 increased, and the β-Sn phase of the shear fracture structure decreased, confirming that the fracture was located in the middle of the IMC at the cathode interface. Additionally, the fracture mode presented a mix of toughness and brittleness. As shown in Figure 12c, the current density increased to 1.1×10^4 A/cm^2 under the action of increasing Joule heating and electronic wind. At this stage, the large spherical dimple inside the shear fracture almost disappeared, and a secondary crack appeared. The fracture was mainly composed of large cleavage facets and tear ridges, and the whole fracture looked relatively smooth and flat. Based on the EDS spectroscopic analysis of the C region presented in Figure 12c, the structure of the shear fracture was almost completely dissolved as the Cu_6Sn_5 phase, mainly the Cu_3Sn phase, and the fracture position shifted from the middle of the cathode interface IMC to the Cu_3Sn interface at the root of the cathode interface IMC. The fracture pattern then changed from ductile fracture to brittle fracture. The void density in the cathode region also increased, resulting in defects such as voids and cracks, which reduced the shear strength of the solder joint, thereby significantly reducing its reliability. The fracture pathways of the solder joints at the three different current density stages are shown in Figure 13.

4. Conclusions

This paper centers on the Sn2.5Ag0.7Cu0.1RE/Cu brazed joints, devising and fabricating electromigration devices and specimens to explore their electromigration characteristics across diverse temperatures and current densities.

1. The electromigration device and specimen designed and manufactured in the present study can meet the requirements for Sn2.5Ag0.7Cu0.1RE/Cu in a constant-temperature oil bath.
2. The electromigration polarity phenomenon of asymmetric growth of IMC at the electromigration interface of Sn2.5Ag0.7Cu0.1RE/Cu solder joints occurred at a temperature of 70 °C and with an angle θ between the c-axis of the β-Sn grain and the current direction of 56.2°. With an increase in temperature to 150 °C, θ gradually decreased to 8.2°, which accelerated the diffusion of Cu atoms and Cu substrate dissolution, and the recrystallization and grain growth of Cu_6Sn_5 grains in the anode region promoted the occurrence of electromigration polarity. Compared with the initial state,

the shear strength decreased to 11 MPa, a decrease of 61.3%, the fracture position shifted from the transition zone of IMC/soldering at the cathode interface to the root of IMC at the cathode interface, and the fracture mode changed from ductile to brittle fracture. In summary, temperature exerts a significant influence on the growth of intermetallic compounds (IMC) at the anode and cathode during electromigration. An increase in temperature intensifies atomic thermal motion and accelerates diffusion. At the anode, the deposition of metal atoms diffusing from the cathode, coupled with enhanced diffusion along grain boundaries, leads to an increase in IMC thickness. Conversely, at the cathode, the accelerated migration of atoms to the anode, combined with an unfavorable microstructure, inhibits IMC growth and reduces its thickness. These findings provide a basis for materials research.

3. At a current density of 5×10^3 A/cm^2, the angle θ between the c-axis and the current direction of the β-Sn grain was 44.8°, and the interface IMC of the Cu_6Sn_5 grain diameter was 2.1–8.3 μm. Moreover, the current density increased to 1.1×10^4 A/cm^2, and θ gradually decreased by 3.2°. Then, the diffusion of Cu atoms and the melting of Cu substrates accelerated, as did the recrystallization of Cu_6Sn_5 grains in the anode region. Additionally, the increase in grain length and diameter accelerated from 6.8 μm to 31.9 μm, which promoted the occurrence of electromigration polarity. Compared to the initial state, the shear strength dropped to 11 MPa, representing a decrease of 55.3%, and the fracture position shifted from the transition zone of IMC/soldering at the cathode interface to the root of the IMC at the cathode interface. Lastly, the fracture mode changed from ductile to brittle. In summary, as the current density increases, the electron wind force strengthens, intensifying electromigration. The electron wind drags metal atoms, like Cu, from the cathode to the anode. In the anode, the additional migrating atoms and accelerated grain boundary diffusion boost IMC growth and thickness. In contrast, the cathode suffers from atom depletion and unfavorable grain boundary diffusion, leading to IMC growth inhibition and eventual failure. This reveals the significant impact of current density on the electromigration-induced IMC growth disparity between the anode and cathode.

Author Contributions: Conceptualization, Y.W. and K.Z.; methodology, Y.W. and K.Z.; software, C.Z. and Y.G.; validation, Y.W., K.Z. and F.H.; investigation, Y.G.; resources, F.H.; data curation, C.Z.; writing—original draft, Y.W.; writing—review and editing, Y.W. and K.Z. All authors have read and agreed to the published version of the manuscript.

Funding: This work was funded by Henan Province International Science and Technology Cooperation Project (Key Project): 241111521400; the Leading Talent in Basic Research in Central Plains: ZYYCYU202012130; Henan Scientific and Technological Research Projects: 242102230048; Provincial and Ministerial Co-construction of Collaborative Innovation Center for Non-Ferrous Metal New Materials and Advanced Processing Technology, Henan Province, China.

Data Availability Statement: The original contributions presented in the study are included in the article, further inquiries can be directed to the corresponding author.

Conflicts of Interest: The authors declare no conflicts of interest.

References

1. Wang, F.; Chen, H.; Huang, Y.; Liu, L.; Zhang, Z. Recent progress on the development of Sn–Bi based low-temperature Pb-free solders. *J. Mater. Sci. Mater. Electron.* **2019**, *30*, 3222–3243. [CrossRef]
2. Xu, J.; Cai, C.; Pham, V.; Pan, K.; Wang, H.; Park, S. A Comprehensive Study of Electromigration in Lead-free Solder Joint. In Proceedings of the 2020 IEEE 70th Electronic Components and Technology Conference (ECTC), the Cosmopolitan of Las Vegas, Las Vegas, NV, USA, 26–29 May 2020.
3. Wang, S.; Tian, Y. The state of art on the micro-joining and nano-joining technologies. *Mater. Sci. Technol.* **2017**, *25*, 1–5.

4. Yang, D.S.; Zhang, H.; Feng, J.Y.; Sa, Z.C.; Wang, C.X.; Tian, Y.H. Research progress on micro-nano connection technology and failure behavior of electronic packaging. *J. Weld. Soc.* **2022**, *43*, 126–136+169.
5. Xue, S.B.; He, P. *Microelectronic Welding Technology*; China Machine Press: Beijing, China, 2012.
6. Sun, F.L.; Wang, J.B.; Liu, Y. Electromigration behavior of Sn Ag Cu-Bi-Ni lead free micro soldering joints. *J. Harbin Inst. Technol.* **2012**, *17*, 1–4.
7. He, H.W.; Xu, G.C.; Guo, F. Advances in electromigration reliability of lead-free soldering materials. *Electron. Compon. Mater.* **2008**, *27*, 6–8.
8. Wu, Y.P.; Zhang, J.S.; Wu, F.S.; An, B. Electromigration of Sn Ag Cu bump interconnects. *J. Semicond.* **2006**, *27*, 1136–1140.
9. Zhang, C.; Zhang, K.K.; Gao, Y.J.; Wang, Y.M.; Hou, R.Q. Study on Ni-GNSs enhanced Sn2.5Ag0.7Cu0.1RE/Cu solder joints β-Sn grain orientation and interfacial IMC growth kinetics under constant temperature thermomigration. *Mater. Charact.* **2023**, *205*, 113263. [CrossRef]
10. Chen, W.J.; Lee, Y.; Wu, T.Y.; Chen, T.C.; Hsu, C.H.; Lin, M.T. Effects of Electrical Current and External Stress on the Electromigration of Intermetallic Compounds Between the Flip-Chip Solder and Copper Substrate. *J. Electron. Mater.* **2018**, *47*, 35–48. [CrossRef]
11. Li, M.Y.; Chang, H. In situ electromigration IMC evolution of Sn Ag Cu lead-free soldered joints. *Electron. Compon. Mater.* **2011**, *30*, 58–60.
12. Chellvarajoo, S.; Abdullah, M.Z.; Khor, C.Y. Effects of diamond nanoparticles reinforcement into lead-free Sn-3.0Ag-0.5Cu solder pastes on microstructure and mechanical properties after reflow soldering process. *Mater. Des.* **2015**, *82*, 206–215. [CrossRef]
13. Han, Y.D.; Jing, H.Y.; Nai, S.M.L.; Xu, L.Y.; Tan, C.M. Interfacial reaction and shear strength of Ni-coated carbon nanotubes reinforced Sn–Ag–Cu solder joints during thermal cycling. *Intermetallics* **2012**, *31*, 72–78. [CrossRef]
14. Zuo, Y.; Ma, L.M.; Lu, Y. The effects of thermal cycling on electro migration behaviors in lead-free solder joints. In Proceedings of the 13th International Conference On Electronic Packaging Technology and High Density Packaging, Guilin, China, 13–16 August 2012; pp. 1068–1071.
15. Wang, H.; Zhang, H.; Ma, L.; Yang, J.; Wang, J. Effect of temperature on electromigration in Cu interconnects with different damascene structures. *J. Electron. Mater.* **2018**, *47*, 3615–3623.
16. Liu, X.; Zhang, X.; Yang, Y.; Li, J.; Li, X.; Zhang, Y. Effect of temperature on the interfacial morphology and electromigration behavior of the Cu/Sn-8.5Zn-3Bi/Cu solder joint. *J. Mater. Sci. Mater. Electron.* **2019**, *30*, 13119–13131.
17. Liu, C.; Sun, M.; Wang, J.; Zhao, W.; Sun, L. Temperature effect on electromigration of Sn-3.0Ag-0.5Cu solder joints under high current density. *J. Mater. Sci. Mater. Electron.* **2021**, *32*, 14829–14840.
18. Li, W.; Li, J.; Zhang, J.; Tian, J.; Shi, J.; Liu, Y. Temperature dependence of electromigration in Cu/low-k interconnects. *Microelectron. Reliab.* **2018**, *89*, 152–158.
19. Hsu, Y.C.; Chou, C.K.; Liu, P.C.; Chen, C.; Yao, D.J. Electromigration in Pb-free SnAg3.8Cu0.7 solder stripes. *J. Appl. Phys.* **2005**, *98*, 033523. [CrossRef]
20. Jiang, N.; Zhang, L.; Xiong, M.Y. Research progress on electromigration of lead-free interconnect soldering joints for electronic packaging. *Electron. Compon. Mater.* **2019**, *38*, 1–8.
21. Fu, X.; Liu, M.; Xu, K. The In-Situ Observation of Grain Rotation and Microstructure Evolution Induced by Electromigration in Sn-3.0Ag-0.5Cu Solder Joints. *Materials* **2020**, *23*, 5497. [CrossRef] [PubMed]
22. Chen, J.Q.; Guo, J.D.; Liu, K.L. Dependence of electromigration damage on Sn grain orientation in Sn–Ag–Cu solder joints. *J. Appl. Phys.* **2013**, *114*, 153509. [CrossRef]
23. Zhang, C.; Zhang, K.K.; Gao, Y.J.; Wang, Y.M. Study on Microstructure and Mechanical Properties at Constant Electromigration Temperature of Sn2.5Ag0.7Cu0.1RE0.05Ni-GNSs/Cu Solder Joints. *Materials* **2023**, *16*, 2626. [CrossRef]
24. Yao, W.; Basaran, C. Damage mechanics of electromigration and thermomigration in lead-free solder alloys under alternating current: An experimental study. *Int. J. Damage Mech.* **2014**, *23*, 203–221. [CrossRef]
25. Wang, F.J.; Zhou, L.L.; Wang, X.J. Microstructural evolution and joint strength of Sn-58Bi/Cu joints through minor Zn alloying substrate during isothermal aging. *J. Alloys Compd.* **2016**, *688*, 639–648. [CrossRef]
26. Liu, H.Y.; Zhu, Q.S.; Wang, Z.G. Effects of Zn addition on electromigration behavior of Sn-1Ag-0.5Cu solder interconnect. *J. Mater. Sci.-Mater. Electron.* **2013**, *24*, 211–216. [CrossRef]
27. Huang, M.L.; Zhao, J.F.; Zhang, Z.J. Role of diffusion anisotropy in beta-Sn in microstructural evolution of Sn-3.0Ag-0.5Cu flip chip bumps undergoing electromigration. *Acta Mater.* **2015**, *100*, 98–106. [CrossRef]
28. Lee, K.; Kim, K.S.; Tsukada, Y. Effects of the crystallographic orientation of Sn on the electromigration of Cu/Sn-Ag-Cu/Cu ball joints. *J. Mater. Res.* **2011**, *26*, 467–474. [CrossRef]
29. Huang, M.L.; Zhao, J.F.; Zhang, Z.J. Dominant effect of high anisotropy in beta-Sn grain on electromigration-induced failure mechanism in Sn-3.0Ag-0.5Cu interconnect. *J. Alloys Compd.* **2016**, *678*, 370–374. [CrossRef]
30. Lin, J. Microstructure and mechanical properties of SnAg0.5CuZn0.1Ni/Cu soldered joint. *Spec. Cast. Nonferrous Alloys* **2016**, *36*, 985–988.

31. Huo, F.P.; Jin, Z.; Han, D.L.; Li, J.H.; Zhang, K.K.; Nishikawa, H. Novel interface regulation of Sn1.0Ag0.5Cu composite solders reinforced with modified ZrO2: Microstructure and mechanical properties. *J. Mater. Sci. Technol.* **2022**, *125*, 157–170. [CrossRef]
32. Guo, F.; Xu, G.C.; He, H.W. Electromigration behaviors in Sb particle-reinforced composite eutectic Sn Ag Cu solder joints. *J. Mater. Sci.* **2009**, *44*, 5595–5601. [CrossRef]
33. Huang, Y.T.; Hsu, H.H.; Wu, A.T. Electromigration-induced back stress in critical solder length for three-dimensional integrated circuits. *J. Appl. Phys.* **2014**, *115*, 6. [CrossRef]
34. Li, S.D.; Basaran, C. Effective diffusivity of lead free solder alloys. *Comput. Mater. Sci.* **2009**, *47*, 71–78. [CrossRef]
35. Tasooji, A.; Lara, L.; Lee, K. Effect of grain boundary misorientation on electromigration in lead-free solder joints. *J. Electron. Mater.* **2014**, *43*, 4386–4394. [CrossRef]
36. Shen, Y.A.; Chen, C. Effect of Sn grain orientation on formation of Cu_6Sn_5 intermetallic compounds during electromigration. *Scr. Mater.* **2017**, *128*, 6–9. [CrossRef]